Hindawi Publishing Corporation
Journal of Nanomaterials
Volume 2016, Article ID 7315821, 8 pages
http://dx.doi.org/10.1155/2016/7315821

Research Article

Continuous Size-Dependent Sorting of Ferromagnetic Nanoparticles in Laser-Ablated Microchannel

Yiqiang Fan,[1] Feng Gao,[1] Huawei Li,[2] Gang Tang,[1] Jian Zhuang,[1] and Bo Yu[3]

[1]*College of Mechanical and Electrical Engineering, Beijing University of Chemical Technology, Beijing, China*
[2]*Department of Mechanical and Industrial Engineering, University of Toronto, Toronto, ON, Canada*
[3]*School of Mechanical and Electrical Engineering, Nanjing Forestry University, Nanjing, China*

Correspondence should be addressed to Gang Tang; tanggang@mail.buct.edu.cn

Received 6 July 2016; Revised 6 October 2016; Accepted 16 October 2016

Academic Editor: Zehra Durmus

This paper reports a low-cost method of continuous size-dependent sorting of magnetic nanoparticles in polymer-based microfluidic devices by magnetic force. A neodymium permanent magnet was used to generate a magnetic field perpendicular to the fluid flow direction. Firstly, $FeNi_3$ magnetic nanoparticles were chemically synthesized with diameter ranges from 80 nm to 200 nm; then, the solution of magnetic nanoparticles and a buffer were passed through the microchannel in laminar flow; the magnetic nanoparticles were deflected from the flow direction under the applied magnetic field. Nanoparticles in the microchannel will move towards the direction of high-gradient magnetic fields, and the degree of deflection depends on their sizes; therefore, magnetic nanoparticles of different sizes can be separated and finally collected from different output ports. The proposed method offers a rapid and continuous approach of preparing magnetic nanoparticles with a narrow size distribution from an arbitrary particle size distribution. The proposed new method has many potential applications in bioanalysis field since magnetic nanoparticles are commonly used as solid support for biological entities such as DNA, RNA, virus, and protein. Other than the size sorting application of magnetic nanoparticles, this approach could also be used for the size sorting and separation of naturally magnetic cells, including blood cells and magnetotactic bacteria.

1. Introduction

Magnetic nanoparticles have been widely used as the carrier in the biosensing and biomedical systems [1–3]. Preparing uniformly sized magnetic nanoparticles is crucial, since magnetic and chemical properties of magnetic nanoparticles not only rely on chemical composition but also rely on the size and shape of the nanoparticles [4–7]. Moreover, in order to coat or bind the biological entity on magnetic nanoparticles, the dimension of the nanoparticles needs to be controlled to match the size of the biological entities, for example, virus (20 nm–450 nm), protein (5 nm–50 nm), and gene (2 nm wide with the length of 10 nm–100 nm) [8]. The current research on controlling the size of nanoparticles usually involves complex chemical reactions with a long reaction time [9–12]. Therefore, a more accessible method of sizing the nanoparticles is desired. In this study, we propose a simple and rapid method for continuous size sorting of magnetic nanoparticles as part of the postsynthesis treatment process, and ferromagnetic nanoparticles were used to demonstrate this new and low-cost approach.

Over the last several years, polymer-based microfluidic devices have developed rapidly, which have been widely used in many applications in the chemical and biological fields [13, 14]. Microfluidic devices provide a rapid, sensitive, and high-throughput platform for chemical or biological reactions and detections with a relatively rapid and low-cost process. In this study, we fabricated a poly(methyl methacrylate) (PMMA) based microfluidic device with the laser-ablated microchannels. This microfluidic device provides a low-cost platform for the continuous flow size sorting of nanoparticles with the applied inhomogeneous magnetic field.

Size sorting and separation of micro/nanoparticles have been widely studied with several approaches, including size

Table 1: Comparison between the methods of continues flow magnetic particles separation.

Method	Material for microfluidic devices	Microchannel fabrication method	Fabrication cost	Upper and lower size of particles	Type of magnet	Number of output ports
Pamme and Manz [32]	Soda line glass	Direct UV laser writing	Medium	2.0/6.0 μm	Permanent NdFeB	16
Peyman et al. [33]	Glass	Photolithography	High	2.0/22.0 μm	Permanent NdFeB	12
Kim and Park [34]	PDMS	Photolithography	High	1.0/1.0 μm	Permanent NdFe35	2
Yung et al. [35]	PDMS	Photolithography	High	1.0/1.0 μm	Electromagnet	4
The proposed method	PMMA	Direct CO_2 laser writing	Low	80/200 nm	Permanent NdFeB	3

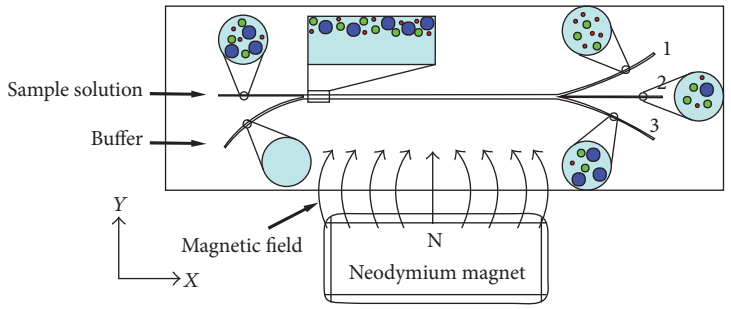

Figure 1: Schematic of the microfluidic device used for magnetic nanoparticles size sorting with neodymium magnet (nanoparticles are not to scale). The sample solution with nanoparticles and buffer enter the microfluidics chip from two inlet ports while the magnetic nanoparticles were deflected and were collected at various output ports.

sorting or separation using magnetic field [15–17], chromatography [18–20], plasmon resonances [21, 22], density gradient centrifugation [23–25], electrophoresis [26–28], and selective precipitation [29–31]. The separation of small particles with an external magnetic field in microchannels was studied by several researchers. Pamme and Manz firstly used the magnetophoresis for the continuous flow separation of magnetic microparticles in the glass microfluidics device [32]. Peyman et al. then introduced the multistep continuous flow separation procedures of microparticles for biochemical applications [33]. Kim and Park developed a microfluidic device for the separation of superparamagnetic nanoparticles in order to detect the target analytes [34]. Yung et al. fabricated a PDMS (polydimethylsiloxane) based micromagnetic-microfluidic blood cleansing device to remove fungi (attached with magnetic microparticles) from contaminated blood [35]. However, most of these methods used photolithography method for the fabrication of glass or PDMS based microfluidic devices, which requires cleanroom environment with highly sophisticated microfabrication instruments.

In this proposed method, the CO_2 laser ablation was used for the fabrication of PMMA based microfluidics device for nanoparticle separation, the whole fabrication process is relatively of low cost and has no requirement of the cleanroom environment. The comparison between this proposed method and other methods is shown in Table 1. It can be concluded from the table that the proposed method has great advantages including low fabrication cost and the ability of size sorting smaller particles (80–200 nm). Based on the previous theoretical studies [36], the minimum diameter of the nanoparticles that can be separated is ~50 nm, when this proposed method is used. Nanoparticles smaller than 50 nm will be significantly influenced by the thermal diffusion and Brownian motion, which may overcome drag force from the magnetic field.

2. Theory

The schematic of the microfluidic device used for the nanoparticles size sorting is shown in Figure 1. The dimension for the microchannel is relatively small (~200 μm), which results in a very low ($\ll$2000) Reynolds number (Re) of the fluid inside the microchannel will proceed as laminar without turbulence mixing. The magnetic field was sourced from a neodymium magnet (NdFeB magnet), and the direction of magnetic field was perpendicular to the direction of the fluid flow.

The reason for using neodymium magnet is that it has a strong energy to easily push the flux into the microfluidics channel under the room temperature and also has a good resistance to demagnetization and corrosion. As a famous ferromagnetic material, neodymium magnet is easily accessible with relatively low cost.

As shown in Figure 1, the sample solution ($FeNi_3$ nanoparticles in DI water) and buffer (DI water) will enter

the microfluidics chip from two separate inlet ports, and these two streams will join in the main channel. With the principle of laminar flow, these two flows will proceed in parallel in the main channel (illustrated in the square shape insert in Figure 1) as the viscous effects dominate over the inertial effects. The ferromagnetic nanoparticles in the microchannel will interact with the external magnetic field and deflect the nanoparticles from the flow direction.

To analyze the motion of the nanoparticles in the microfluidics channel, the velocity composition of a single nanoparticle is shown in Figure 2. As described in this figure, the velocity of a single magnetic nanoparticle ($\mathbf{v}_t$) moving in the microchannel will be influenced by the sum of two aspects: hydrodynamic force ($\mathbf{v}_{\text{hydr}}$) from the fluid flow and the magnetic field ($\mathbf{v}_{\text{mf}}$) from the neodymium magnet. The detailed relations of velocity and force are described with the following equations:

$$\mathbf{v}_t = \mathbf{v}_{\text{hydr}} + \mathbf{v}_{\text{mf}}, \tag{1}$$

$$\mathbf{F}_{\text{mf}} = \frac{1}{2}\frac{v_{\text{m}}\Delta\chi_{\text{m}}}{\mu_0}\nabla\mathbf{B}^2, \tag{2}$$

$$\mathbf{v}_{\text{mf}} = \frac{\mathbf{F}_{\text{mf}}}{6\pi\eta r} = \frac{v_{\text{m}}\Delta\chi_{\text{m}}}{12\pi\eta r\mu_0}\nabla\mathbf{B}^2, \tag{3}$$

$$\mathbf{v}_{\text{mf}} \propto r^2\Delta\chi_{\text{m}}. \tag{4}$$

The magnetic force ($\mathbf{F}_{\text{mf}}$) on a single magnetic nanoparticle in the microfluidic channel can be described with (2) [37], where v_{m} is the volume of the nanoparticles, $\Delta\chi_{\text{m}}$ is the magnetic susceptibility difference between the nanoparticles and the fluid (DI water, in our case), $\mathbf{B}$ is the magnetic field applied from a permanent magnet, and μ_0 is the permeability in vacuum. The velocity vector of a single nanoparticle was influenced by the magnetic field; $\mathbf{v}_{\text{mf}}$ can be then described as the magnetic force over the viscous drag force in (3). As described by (3), for a given magnetic field and fluid, $\mathbf{v}_{\text{mf}}$ only depends on the radius of the nanoparticles, r, and magnetic susceptibility, $\Delta\chi_{\text{m}}$ (shown in (4)).

According to (4), bigger nanoparticles deflect more from the fluid flow direction, which indicates the basic working principle of our microfluidic device for the continuous size sorting of nanoparticles. Nanoparticles with different size distributions were collected at the three outlet ports (shown in Figure 1) due to different deflections during the propagation inside the microchannel.

Using COMSOL Multiphysics, the magnetic flux density ($\mathbf{B}$) distribution generated from a neodymium magnet (shown in Figure 1) was also numerically simulated for the analysis of the magnetic field gradient. Figure 3 shows the magnetic flux density at two directions. From the simulation results, when an inhomogeneous magnetic field is applied, the magnetic field gradient is generated in the y-direction (Figure 3(a)), and the magnetic field gradient is the source of magnetic force applied on the ferromagnetic nanoparticles as shown in (2). The ferromagnetic nanoparticles, which are moving with the fluid flow along the x-direction, will be deflected and start moving in the y-direction due to the drag force created by the magnetic gradient. The magnetic gradient in the z-direction (Figure 3(b)) can be ignored because of the low depth (~100 μm) of the microchannels.

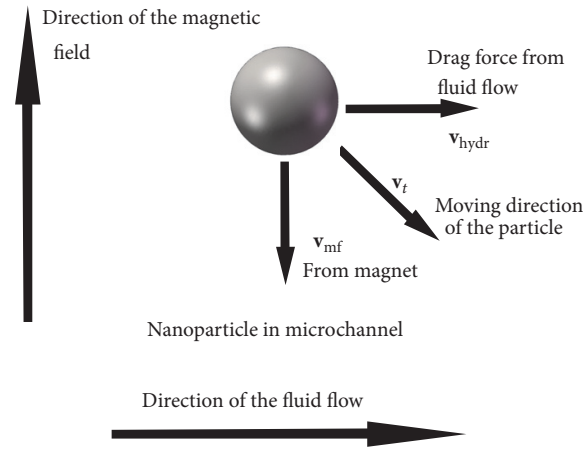

Figure 2: Velocity composition of nanoparticle in microfluidics channel and the velocity of a single magnetic nanoparticle $\mathbf{v}_t$ composite velocity sourced from hydrodynamic force $\mathbf{v}_{\text{hydr}}$ and the velocity sourced from the magnetic field $\mathbf{v}_{\text{mf}}$.

3. Fabrication Process of the Microfluidic Device and Experimental Results

The synthesis process of $FeNi_3$ nanoparticles was as follows: iron(II) chloride ($FeCl_2$) and nickel(II) chloride ($NiCl_2$) were dissolved in DI water followed by the addition of polyethyl glycol (PEG) with a formula weight (FW) of 6000. Then sodium hydroxide (NaOH) was added to solution to adjust the pH value within the range of 12-13. After that, hydrazine hydrate was added to the suspension. The reaction continued for 24 hours under room temperature (24°C) to obtain the $FeNi_3$ nanoparticles. The SEM (scanning electron microscope) image of the synthesized $FeNi_3$ nanoparticles is provided in Figure 4 (Quanta 600 FEG). The size distribution before and after the size sorting of these nanoparticles will be discussed in the following sections.

The fabrication process of the microfluidic devices is shown in Figure 5. The process starts with fabricated microchannels on PMMA with direct laser ablation. A commercial CO_2 laser system (Universal PL6.75) was used to thermally ablate the microchannels on a 1.5-mm thick PMMA (Lucite cast acrylic sheet) substrate (Figure 5(a)). The power setting of the laser was 37.5 W with a scan speed of 150 mm/s in the pulse mode of 1000 PPI (points per inch). During the laser ablation of microchannels, the absorption of laser power will cause the PMMA surface to melt, decompose, and finally vaporize to form the microchannels. The width of the microchannels was 200 μm with a depth of 100 μm (measured with profilometer).

The next step was thermal-compression bonding [38]. In order to seal the microchannels on PMMA substrate, another piece of 1.5-mm thick PMMA, with through holes for inlet and outlet ports, was bonded to the substrate (Figure 5(b)). This thermal-compression bonding (using INSTRON Dual

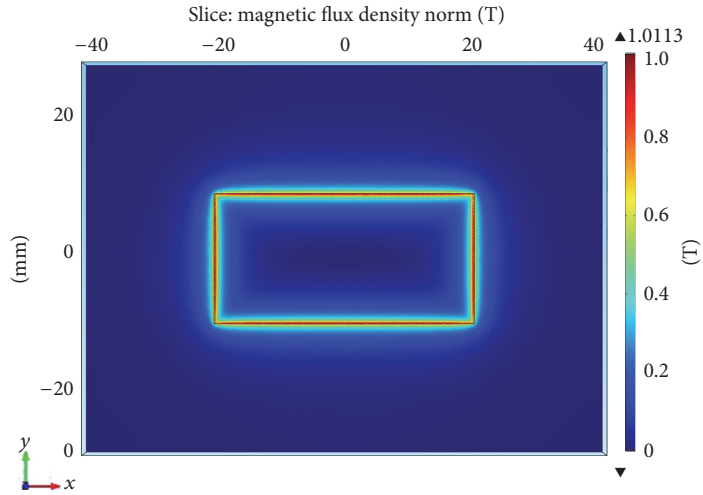

(a) Plot on X-Y plane

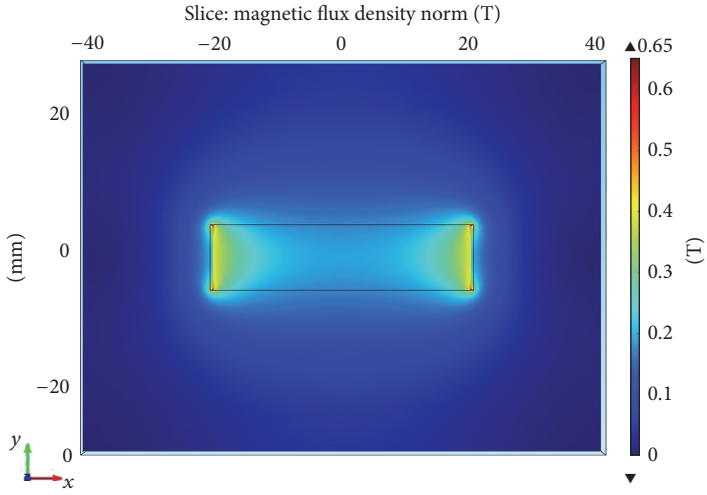

(b) Plot on X-Z plane

Figure 3: Simulation results for the 3D magnetic flux density of the neodymium magnet. (a) The magnetic flux density distribution on X-Y plane. (b) The magnetic flux density distribution on X-Z plane.

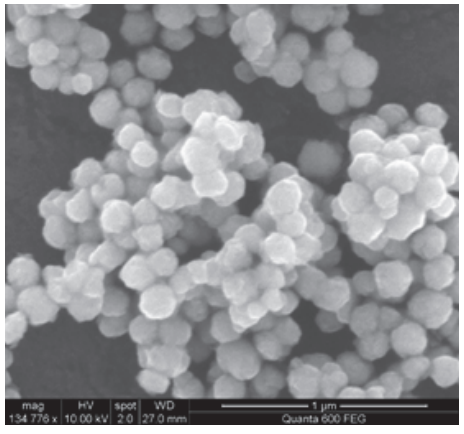

Figure 4: SEM image of the synthesized $FeNi_3$ nanoparticles. By measuring the size of each nanoparticle, the distribution of the magnetic nanoparticles from each outlet port could be obtained.

Column Testing Systems) was conducted at 140°C with a compression pressure of 0.4 MPa for 1 hour. The final step was piping: five plastic pipes (Tygon, Saint-Gobain Performance Plastics) were connected at two inlet ports and three outlet ports. The microfluidic devices were now ready for the following nanoparticles size sorting test. The whole fabrication cost for each chip is lower than 10 US dollars.

The system setup for the size sorting process of the ferromagnetic nanoparticles is shown in Figure 6. Using a syringe pump (Fusion 200), the $FeNi_3$ solution ($FeNi_3$ powder in DI water, 10 mg/L) and buffer (DI water) were pumped into the microfluidics chip with the same rate of 200 μL/min through two inlet ports. The neodymium magnet was placed with an edge-to-edge distance of 5 mm from the microfluidics chip. Three centrifuge tubes (polystyrene, CELLSTAR) were connected to the three outlet ports to collect the output samples.

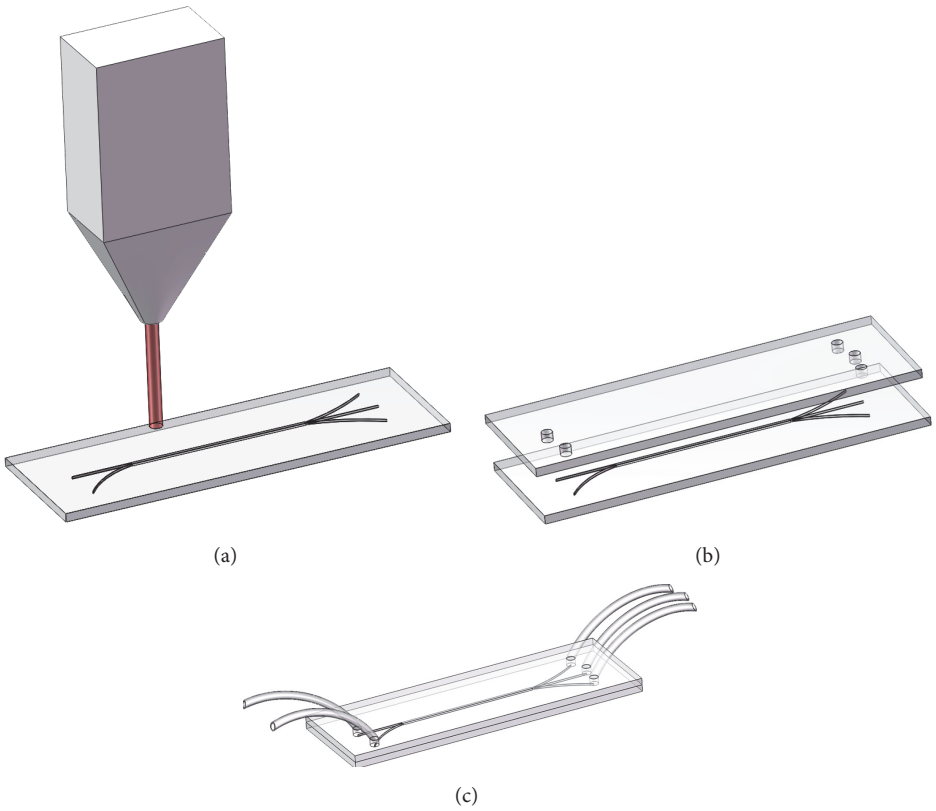

FIGURE 5: Fabrication processes of the microfluidic device. The fabrication process included the laser ablation of microchannels on PMMA substrate (a), the thermal-compression bonding processing to seal the microchannel (b), and the piping (c).

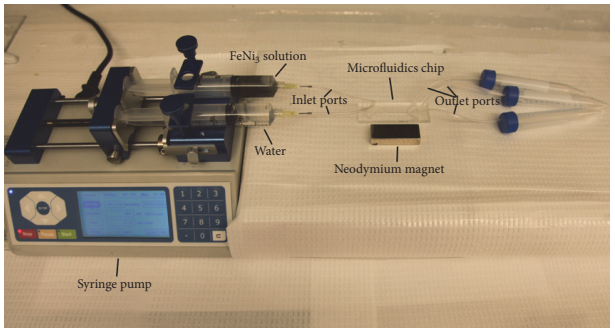

FIGURE 6: System setup for the $FeNi_3$ nanoparticles size sorting process, including the syringe pump, microfluidics chip, neodymium magnet, and centrifuge tubes for sample collection.

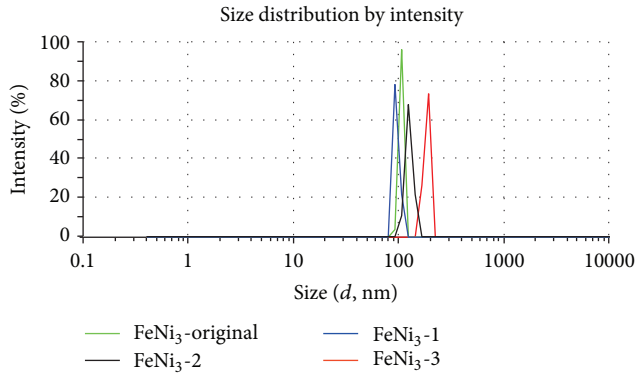

FIGURE 7: Size distribution results from three outlet ports obtained from the nanoparticle analyzer.

4. Result and Discussion

The size sorting result of the $FeNi_3$ nanoparticles was characterized by two means. The first method used the nanoparticle analyzer (Zetasizer Nano ZSP, Malvern) to analyze the size distribution of the $FeNi_3$ nanoparticles collected from three outlet ports. The second method used SEM (Quanta 600 FEG) to take images of the samples from three outlet ports and with the help of image processing software to analyze the size distribution of these nanoparticles. Both of these methods showed that the average diameters of the nanoparticles from the three outlets were different: the closer the outlet ports to the neodymium magnet, the larger the nanoparticles.

Figure 7 shows the size distribution plot from the nanoparticle analyzer. The nanoparticle analyzer for measuring size is based on dynamic light scattering (DLS). Briefly, the principle of the DLS is as follows: in the water solution, the nanoparticles are in a random motion called Brownian motion. When the light scattered from the nanoparticles

Table 2: Size distribution results from three outlet ports obtained by nanoparticle analyzer.

Output ports	Distribution peak (d, nm)	Standard deviation (d, nm)
Original solution before size sorting	125	10
Output port 1	94	6
Output port 2	105	3
Output port 3	183	8

in the solution was enhanced, due to the random motions of the nanoparticles, the intensity of the scattered light has a time-dependent fluctuation. This fluctuation is directly related to the rate of diffusion of nanoparticles in the solvent which depends on the nanoparticles' hydrodynamic radius. With the detection of fluctuation using laser and photon detector, the hydrodynamic radius of the nanoparticles can be calculated.

Table 2 shows the peak of the distribution and the standard deviation for each output port as well as the original $FeNi_3$ nanoparticle solution without size sorting. Clearly, the peaks of the size distribution for the three outlet ports are different. From the position of the three outlet ports (shown in Figure 1), we conclude that larger nanoparticles will be attracted and deflected more than smaller nanoparticles inside the main channel, which will lead to the distribution difference at the three outlet ports.

Besides the diameter data of the nanoparticles, Table 1 also shows that the standard deviation of the three outlet ports is much smaller than the standard deviation of the original solution. This result indicates that, after the size sorting process, the size distribution of nanoparticles was narrowed.

Another measurement process was also conducted to verify the result from nanoparticle analyzer. Ferromagnetic nanoparticle samples from each output port were sent for SEM imaging. Then, software (Nano Measurer 1.2.5), based on pixel counting, was used to measure the size of nanoparticles from the SEM images (i.e., Figure 4). All the statistical analysis was performed using PASW Statistics 18 software. The histograms of diameter distribution for nanoparticles from each of the three outlet ports are shown in Figure 8. Each group has a sample volume of 500–700 (500–700 nanoparticles were measured for each group), and therefore the results are statistically reliable. Table 3 shows the detailed data analysis for each group of samples from the three outlet ports. These data clearly demonstrate that the results from this method highly correspond to the measurement results from the nanoparticle analyzer; that is, the outlet port nearest to the neodymium magnet has the largest average diameter of nanoparticles.

Comparing the data from the two measuring methods shown in Tables 2 and 3, although the general trend is the same, the exact data is slightly shifted. This difference is a result of the two totally different measuring methods. For the nanoparticle analyzer, the dynamic light scattering of the

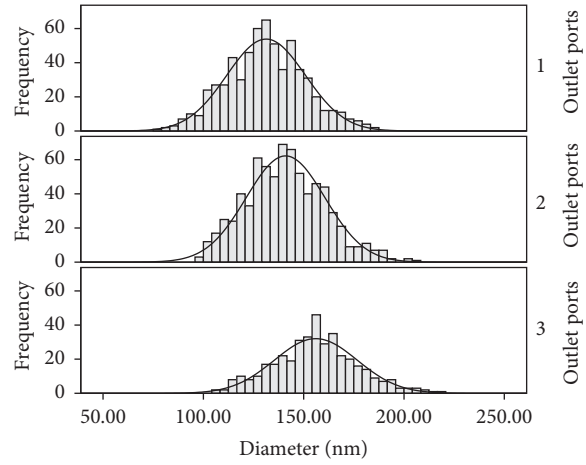

Figure 8: Size distribution results from three outlet ports obtained by analyzing the SEM images.

sample solution was used to measure the size of samples, and the final measured nanoparticle diameter was based on the hydrodynamic radius (stokes radius), which not only depends on the size of the nanoparticles but also depends on the solvent (DI water in this case). The second method measured the actual diameter of the nanoparticles based on pixel counting of the SEM images with the reference of scale bar provided in the SEM images. Based on this, we can conclude that the measurement results from two methods were corresponding with each other, although the exact data was slightly different.

5. Conclusion

In this paper, a low-cost polymer-based microfluidic device was used for the continuous size sorting of magnetic nanoparticles. The polymer microfluidic device was fabricated by laser ablation which is simple and rapid. Ferromagnetic nanoparticles were used to demonstrate this proposed method. The magnet field was generated by a neodymium magnet, and nanoparticles inside the microchannel deflected from the flow direction as a result of this applied magnetic field; the deflection depends on the size of the nanoparticles. After sorting the nanoparticles, the samples from each output port were characterized by both a nanoparticle analyzer and software analysis based on SEM images. The data from the three outlet ports show that the distribution of nanoparticles has different peak sizes and the outlet port nearest to the neodymium magnet has the largest average size of nanoparticles, whereas the port furthest from the magnet has the smallest. The size distributions for all three outlet ports have been compared with the original solution.

This research provides a low-cost and rapid way of continuous size sorting of magnetic nanoparticles with polymer-based microfluidic device. The proposed technique has lots of potential applications for preparing evenly distributed magnetic nanoparticles as the carrier for biological and chemical entities.

Table 3: Size distribution results from three outlet ports obtained by analyzing the SEM images.

	Descriptive statistics				
	N	Minimum	Maximum	Mean	Std. deviation
Diameter group 1	635	79 nm	185 nm	131 nm	19.60
Diameter group 2	736	100 nm	206 nm	141 nm	19.65
Diameter group 3	498	106 nm	219 nm	156 nm	20.66

Competing Interests

The authors declare that there is no conflict of interests regarding the publication of this paper.

Acknowledgments

This work was supported by the CNPC Innovation Foundation (2014D-5006-0104) and Fundamental Research Funds for the Central Universities (ZY1613).

References

[1] J. Wang, Z. Chen, Z. Li, and Y. Yang, "Magnetic nanoparticles based dispersive micro-solid-phase extraction as a novel technique for the determination of estrogens in pork samples," *Food Chemistry*, vol. 204, pp. 135–140, 2016.

[2] W. Wang, P. Ma, H. Dong et al., "A magnetic nanoparticles relaxation sensor for protein–protein interaction detection at ultra-low magnetic field," *Biosensors & Bioelectronics*, vol. 80, pp. 661–665, 2016.

[3] Y. Jin, F. Liu, C. Shan, M. Tong, and Y. Hou, "Efficient bacterial capture with amino acid modified magnetic nanoparticles," *Water Research*, vol. 50, pp. 124–134, 2014.

[4] A. Bahadorimehr, Z. Rashemi, and B. Y. Majlis, "The influence of magnetic nanoparticles' size on trapping efficiency in a microfluidic device," *Materials Science & Engineering A*, vol. 486, pp. 381–388, 2015.

[5] F. Li, W. Wu, A. Ning, and J. Wang, "Surface functionalization and magnetic motion of hydrophobic magnetic nanoparticles with different sizes," *International Journal of Chemical Reactor Engineering*, vol. 13, no. 1, pp. 113–118, 2015.

[6] A. Albanese, P. S. Tang, and W. C. W. Chan, "The effect of nanoparticle size, shape, and surface chemistry on biological systems," *Annual Review of Biomedical Engineering*, vol. 14, pp. 1–16, 2012.

[7] N. Ma, C. Ma, C. Li et al., "Influence of nanoparticle shape, size, and surface functionalization on cellular uptake," *Journal of Nanoscience & Nanotechnology*, vol. 13, no. 10, pp. 6485–6498, 2013.

[8] Q. A. Pankhurst and J. Dobson, "Applications of magnetic nanoparticles in biomedicine," *Journal of Physics D: Applied Physics*, vol. 36, no. 13, p. R167, 2003.

[9] H. Wang, J. Li, X. Kou, and L. Zhang, "Synthesis and characterizations of size-controlled $FeNi_3$ nanoplatelets," *Journal of Crystal Growth*, vol. 310, no. 12, pp. 3072–3076, 2008.

[10] A. Bandhu, S. Sutradhar, S. Mukherjee, J. M. Greneche, and P. K. Chakrabarti, "Synthesis, characterization and magnetic property of maghemite (γ-Fe_2O_3) nanoparticles and their protective coating with pepsin for bio-functionalization," *Materials Research Bulletin*, vol. 70, pp. 145–154, 2015.

[11] D. Ling, N. Lee, and T. Hyeon, "Chemical synthesis and assembly of uniformly sized iron oxide nanoparticles for medical applications," *Accounts of Chemical Research*, vol. 48, no. 5, pp. 1276–1285, 2015.

[12] N. G. Bastús, F. Merkoçi, J. Piella, and V. Puntes, "Synthesis of highly monodisperse citrate-stabilized silver nanoparticles of up to 200 nm: kinetic control and catalytic properties," *Chemistry of Materials*, vol. 26, no. 9, pp. 2836–2846, 2014.

[13] I. Bernacka-Wojcik, P. Lopes, A. Catarina Vaz et al., "Bio-microfluidic platform for gold nanoprobe based DNA detection-application to *Mycobacterium tuberculosis*," *Biosensors and Bioelectronics*, vol. 48, pp. 87–93, 2013.

[14] M. L. Kovarik, P. K. Shah, P. M. Armistead, and N. L. Allbritton, "Microfluidic chemical cytometry of peptide degradation in single drug-treated acute myeloid leukemia cells," *Analytical Chemistry*, vol. 85, no. 10, pp. 4991–4997, 2013.

[15] M. Wierucka and M. Biziuk, "Application of magnetic nanoparticles for magnetic solid-phase extraction in preparing biological, environmental and food samples," *TrAC—Trends in Analytical Chemistry*, vol. 59, pp. 50–58, 2014.

[16] R. R. Shah, T. P. Davis, A. L. Glover, D. E. Nikles, and C. S. Brazel, "Impact of magnetic field parameters and iron oxide nanoparticle properties on heat generation for use in magnetic hyperthermia," *Journal of Magnetism and Magnetic Materials*, vol. 387, pp. 96–106, 2015.

[17] E. R. Essinger-Hileman, E. J. Popczun, and R. E. Schaak, "Magnetic separation of colloidal nanoparticle mixtures using a material specific peptide," *Chemical Communications*, vol. 49, no. 48, pp. 5471–5473, 2013.

[18] B. Franze and C. Engelhard, "Fast separation, characterization, and speciation of gold and silver nanoparticles and their ionic counterparts with micellar electrokinetic chromatography coupled to ICP-MS," *Analytical Chemistry*, vol. 86, no. 12, pp. 5713–5720, 2014.

[19] T. A. Hanley, R. Saadawi, P. Zhang, J. A. Caruso, and J. Landero-Figueroa, "Separation of silver ions and starch modified silver nanoparticles using high performance liquid chromatography with ultraviolet and inductively coupled mass spectrometric detection," *Spectrochimica Acta Part B: Atomic Spectroscopy*, vol. 100, pp. 173–179, 2014.

[20] K. Proulx and K. J. Wilkinson, "Separation, detection and characterisation of engineered nanoparticles in natural waters using hydrodynamic chromatography and multi-method detection (light scattering, analytical ultracentrifugation and single particle ICP-MS)," *Environmental Chemistry*, vol. 11, no. 4, pp. 392–401, 2014.

[21] A. J. Blanch, M. Döblinger, and J. Rodríguez-Fernández, "Simple and rapid high-yield synthesis and size sorting of multibranched hollow gold nanoparticles with highly tunable nir plasmon resonances," *Small*, vol. 11, no. 35, pp. 4550–4559, 2015.

[22] A. Cuche, A. Canaguier-Durand, E. Devaux, J. A. Hutchison, C. Genet, and T. W. Ebbesen, "Sorting nanoparticles with intertwined plasmonic and thermo-hydrodynamical forces," *Nano Letters*, vol. 13, no. 9, pp. 4230–4235, 2013.

[23] Y. J. Shin, E. Ringe, M. L. Personick et al., "Centrifugal shape sorting and optical response of polyhedral gold nanoparticles," *Advanced Materials*, vol. 25, no. 29, pp. 4023–4027, 2013.

[24] F. Bonaccorso, M. Zerbetto, A. C. Ferrari, and V. Amendola, "Sorting nanoparticles by centrifugal fields in clean media," *Journal of Physical Chemistry C*, vol. 117, no. 25, pp. 13217–13229, 2013.

[25] S. Dong, Y. Wang, Y. Tu et al., "Separation of gold nanorods by viscosity gradient centrifugation," *Microchimica Acta*, vol. 183, no. 3, pp. 1269–1273, 2016.

[26] S. Ho, K. Critchley, G. D. Lilly, B. Shim, and N. A. Kotov, "Free flow electrophoresis for the separation of CdTe nanoparticles," *Journal of Materials Chemistry*, vol. 19, no. 10, pp. 1390–1394, 2009.

[27] Z.-S. Gong, L.-P. Duan, and A.-N. Tang, "Amino-functionalized silica nanoparticles for improved enantiomeric separation in capillary electrophoresis using carboxymethyl-β-cyclodextrin (CM-β-CD) as a chiral selector," *Microchimica Acta*, vol. 182, no. 7-8, pp. 1297–1304, 2015.

[28] M. Bouri, R. Salghi, M. Algarra, M. Zougagh, and A. Ríos, "A novel approach to size separation of gold nanoparticles by capillary electrophoresis-evaporative light scattering detection," *RSC Advances*, vol. 5, no. 22, pp. 16672–16677, 2015.

[29] W. Zhao, L. Lin, and I.-M. Hsing, "Nucleotide-mediated size fractionation of gold nanoparticles in aqueous solutions," *Langmuir*, vol. 26, no. 10, pp. 7405–7409, 2010.

[30] S. Pardeshi, R. Dhodapkar, and A. Kumar, "Molecularly imprinted microspheres and nanoparticles prepared using precipitation polymerisation method for selective extraction of gallic acid from Emblica officinalis," *Food Chemistry*, vol. 146, pp. 385–393, 2014.

[31] J. N. Duggan and C. B. Roberts, "Aggregation and precipitation of gold nanoparticle clusters in carbon dioxide-gas-expanded liquid dimethyl sulfoxide," *Journal of Physical Chemistry C*, vol. 118, no. 26, pp. 14595–14605, 2014.

[32] N. Pamme and A. Manz, "On-chip free-flow magnetophoresis: continuous flow separation of magnetic particles and agglomerates," *Analytical Chemistry*, vol. 76, no. 24, pp. 7250–7256, 2004.

[33] S. A. Peyman, A. Iles, and N. Pamme, "Rapid on-chip multi-step (bio)chemical procedures in continuous flow—manoeuvring particles through co-laminar reagent streams," *Chemical Communications*, no. 10, pp. 1220–1222, 2008.

[34] K. S. Kim and J.-K. Park, "Magnetic force-based multiplexed immunoassay using superparamagnetic nanoparticles in microfluidic channel," *Lab on a Chip*, vol. 5, no. 6, pp. 657–664, 2005.

[35] C. W. Yung, J. Fiering, A. J. Mueller, and D. E. Ingber, "Micromagnetic-microfluidic blood cleansing device," *Lab on a Chip*, vol. 9, no. 9, pp. 1171–1177, 2009.

[36] D. Fletcher, "Fine particle high gradient magnetic entrapment," *IEEE Transactions on Magnetics*, vol. 27, no. 4, pp. 3655–3677, 1991.

[37] G. P. Hatch and R. E. Stelter, "Magnetic design considerations for devices and particles used for biological high-gradient magnetic separation (HGMS) systems," *Journal of Magnetism and Magnetic Materials*, vol. 225, no. 1-2, pp. 262–276, 2001.

[38] Y. Fan, H. Li, Y. Yi, and I. G. Foulds, "PMMA to Polystyrene bonding for polymer based microfluidic systems," *Microsystem Technologies*, vol. 20, no. 1, pp. 59–64, 2014.